Title

Raman-based cytopathology: an approach to improve diagnostic accuracy in medullary thyroid carcinoma.

Journal

Biomedical Optics Express, 11(12)

ISSN

2156-7085

Authors

Soares de Oliveira, Marcos A
Campbell, Michael
Afify, Alaa M
et al.

Publication Date

2020-12-01

DOI

10.1364/boe.410359

Peer reviewed

Research Article | Vol. 11, No. 12 / 1 December 2020 / Biomedical Optics Express 6962
Biomedical Optics EXPRESS

Raman-based cytopathology: an approach to improve diagnostic accuracy in medullary thyroid carcinoma

MARCOS A. SOARES DE OLIVEIRA,[1] MICHAEL CAMPBELL,[2] ALAA M. AFIFY,[1] ERIC C. HUANG,[3,4] AND JAMES W. CHAN[1,4,*]

[1]Department of Pathology & Laboratory Medicine, Univ. of California Davis, Sacramento, CA 95817, USA
[2]Department of Surgery, Univ. of California Davis, Sacramento, CA 95817, USA
[3]Department of Pathology, Univ. of Washington, Seattle, WA 98104, USA
[4]ECH and JWC contributed equally as senior authors
*jwjchan@ucdavis.edu

Abstract: Medullary thyroid carcinoma (MTC) is a rare form of thyroid malignancy that can be diagnostically challenging on fine needle aspiration (FNA) cytology. Ancillary tests such as elevated serum or immunohistochemical positive calcitonin have been helpful, yet they can occasionally provide false positive results. In search for an alternative method to improve diagnostic accuracy (DA), we applied hyperspectral Raman spectroscopy to characterize the biochemical composition of single cells from MTC and compared their spectral information to cells from other types of thyroid nodules. Hyperspectral Raman images of 117 MTC single cells from digested tissue were obtained with a line-scan hyperspectral Raman microscope and compared to 127 benign and 121 classic variant of papillary thyroid carcinoma (CVPTC) cells. When principal component analysis and linear discriminant analysis were used to classify the spectral data, MTC cells were differentiated from benign and CVPTC cells with 97% and 99% DA, respectively. In addition, MTC cells exhibited a prominent Raman peak at 1003 cm^{-1}, whose intensity is 84% and 226% greater on average than that observed in benign and CVPTC cells, respectively. When specifically utilizing only this peak as a spectral marker, MTC cells were separated from benign and CVPTC cells with 87% and 95% DA, respectively. As this peak is linked to phenylalanine, which is known to be associated with calcitonin release in thyroid parafollicular cells, the increased intensity further suggests that this Raman peak could potentially be a new diagnostic marker for MTC. Furthermore, preliminary data from MTC cells (n=21) isolated from a simulated FNA procedure provided similar Raman signatures when compared to single cells from digestion. These results suggest that "Raman-based cytopathology" can be used as an adjunct technique to improve the diagnostic accuracy of FNA cytopathology at a single cell level.

1. Introduction

Medullary thyroid carcinoma (MTC) is a rare malignant neuroendocrine neoplasm arising from the parafollicular or calcitonin-producing C cells. Although MTC accounts for only 2–5% of all thyroid cancers in the United States, it is responsible for 8-13% of total deaths with a 10-year survival rate of approximately 50% [1,2]. MTC can be sporadic (70-80% of cases) or familial associated with mutations of the REarranged during Transfection (RET) oncogene. The sporadic form is usually solitary whereas the familial form is typically multicentric and bilateral. When MTC is presented with palpable nodules, 70% and 10% of the patients will have cervical and distant metastasis, respectively [3]. The prognosis of MTC is poor, with a 10-year survival rate for patients with stage IV disease of 21% [4]. Both the cure and survival rates of MTC patients can be significantly affected by an early diagnosis and appropriate surgical treatment [2].

#410359 https://doi.org/10.1364/BOE.410359
Journal © 2020 Received 16 Sep 2020; revised 13 Oct 2020; accepted 19 Oct 2020; published 6 Nov 2020

Biomedical Optics EXPRESS

The majority of clinically worrisome thyroid nodules are evaluated by ultrasound-guided fine needle aspiration (FNA) and interpreted by cytopathologists according to the Bethesda System for Reporting Thyroid Cytopathology [5]. Cytologic interpretation for MTC can be straightforward when all the classic criteria are fulfilled: predominance of spindled, epithelioid, and/or oncocytic cells, "salt and pepper" chromatin, occasional pseudoinclusions, plasmacytoid cytoplasm, and background amyloid [5,6]. However, not all cases will manifest with these features. A common practice is looking for the presence of calcitonin either through markedly elevated serum level (>500 pg/mL) or immunohistochemical positivity in tissue blocks [7]. However, an increase in calcitonin serum levels is also observed in other diseases such as hypercalcemias, hypergastrinemias and neuroendocrine tumors with associated hypercalcitoninemia, suggesting that serum calcitonin level can provide false positive results [8]. In addition, oncocytic cells are known to give nonspecific staining with calcitonin leading to further diagnostic inaccuracy [9]. Hence, a new approach that can provide a rapid, reliable and accurate diagnosis would have a significant clinical impact in the care and management of patients with MTC.

During the last decades, Raman spectroscopy has grown from research laboratories and is increasingly used in medical [10–12], and other cytological applications (e.g. oral and cervical) [13,14]. We previously reported on hyperspectral Raman microscopy being able to identify single cells dissociated from human tissues of benign and papillary carcinoma thyroid nodules with 97% diagnostic accuracy [15]. Hyperspectral Raman images of individual cells were converted into single cell Raman spectra capturing the biochemical composition of the entire cell, which were used as label-free molecular fingerprints for cell identification and differentiation. Spectral differences associated with varying levels of phenylalanine, tryptophan, proteins, lipids, and nucleic acids were observed. Our preliminary results also showed the feasibility of distinguishing other tumor subtypes, including follicular adenoma, follicular carcinoma, and follicular variant of papillary thyroid carcinoma [15]. In the present study, we applied similar principles of hyperspectral Raman microscopy to identify the biochemical composition of single cells from MTC nodules based on their intrinsic Raman spectral signatures.

2. Materials and methods

2.1. Tissue collection

Tissue samples of human thyroid nodules were obtained from the University of California Davis Medical Center Biorepository under an Institutional Review Board approved protocol. All patients were consented prior to study enrollment. Thyroidectomies were processed according to routine surgical pathology with hematoxylin and eosin stain, and the original diagnosis was reconfirmed by a second pathologist to ensure quality assurance of the collected samples. Only nodules that had sufficient residual tissue after diagnostic sampling were included in the study.

Single cells were obtained from the thyroid nodules using a tissue dissociation method that has been described previously [15]. Briefly, the tissue was incubated at 37°C in a collagenase solution for a few hours to digest the tissue and single cells were separated from the larger tissue fragments using a 70 µm pore size nylon mesh. The single cells were then fixed with a 4% paraformaldehyde (PFA) in phosphate buffered saline (PBS) solution, washed by centrifugation several times, and resuspended in fresh PBS solution. Table 1 summarizes the number and types of thyroid nodules used in this study and the number of single cell Raman images that were obtained. Each nodule was obtained from a different patient.

A second method intended to mimic FNA procedure was also applied to obtain single cells from the MTC thyroid nodules. A 27-gauge fine needle attached to a syringe was used to aspirate cells from the nodules, a method similar to in vivo sampling, prior to collagenase digestion. The cells aspirated were released into a PFA solution for cell fixation. After a few minutes, the cells were then washed by centrifugation and resuspended in PBS solution.

Biomedical Optics EXPRESS

Table 1. Number of thyroid nodules and Raman images of single, dissociated cells.

Nodule Type	Number of nodules	Number of Raman images
Medullary thyroid carcinoma	4	117
Benign nodular hyperplasia	5	127
Papillary thyroid carcinoma, classic variant	5	121
Total	**14**	**365**

Cells were analyzed by pipetting the cell solution onto a 1 inch round quartz coverslip (0.15 to 0.18 mm thickness) mounted in a cell chamber holder and placed onto the stage of the Raman microscope. Cells remained immersed in PBS solution for the duration of the spectroscopy measurements.

2.2. Data acquisition

Hyperspectral Raman images of individual cells were obtained using a line-scan Raman microscope as previously described [15]. Figure 1 shows the experimental method for acquiring a hyperspectral Raman image of a cell. The Raman microscope uses a 785 nm wavelength master oscillator power amplifier fiber laser system (Sacher-Laser) as the excitation source. A pair of achromatic spherical lenses is used to expand the laser beam diameter and a narrow 785 nm maxline laser-line clean-up filter (Semrock, LL01-785) is used to ensure monochromatic excitation. An achromatic cylindrical lens (Thorlabs, f = 100 mm) changes the Gaussian beam profile into a line profile, which is imaged by an achromatic spherical lens (Thorlabs, f = 500 mm) to an inverted microscope (Leica, DM IRM) equipped with a motorized flat top translational scan stage (ProScan Prior II) and a 60x 1.2 N.A. water immersion objective lens (Olympus, UPlanSApo). A 785 nm dichroic laser beamsplitter (Semrock, LP02-785RU) is used to direct the laser to the microscope. The length of the line at the sample plane is approximately 50 µm with a diffraction-limited width. The Raman signals generated from the line shaped focal region are collected by the same objective lens, passed through the dichroic beamsplitter, and imaged by an achromatic lens (Thorlabs, f = 125 mm) onto the entrance-slit of the spectrometer (PI Acton, SpectraPro SP2300i). A long pass filter (Semrock, LP02-785RE) is placed in front of the spectrometer. The slit is adjusted to a width of 20 µm. A 600 grooves per mm grating is used to disperse the Raman signals from the line pattern, which is imaged onto a back-illuminated deep-depletion CCD detector (PI Acton, Pixis100). The image of the 50 µm long line is projected onto 100 pixels on the CCD chip. Typical Raman acquisition times per line is 50 seconds, leading to a full hyperspectral Raman image of a single cell within minutes by scanning the cell with a 1 µm step size in the direction perpendicularly to the excitation laser line.

2.3. Data processing

Background removal was performed on the spectra based on an automated iterative polynomial curve-fitting method for background subtraction from biological Raman spectra [15]. Background-free false color Raman images can be generated for each cell by using the area intensities of different Raman peaks, as shown in Fig. 1(d). For the purpose of cell classification, the multidimensional hyperspectral Raman image of an individual cell is converted into a single Raman spectrum that most accurately represents the individual cell by summing up all Raman spectra belonging to the cell, and then normalizing the spectrum to the total area under the curve. Principal component analysis (PCA) and linear discriminant analysis (LDA) techniques were then performed to analyze the Raman spectral data of single cells. The PCA-LDA model uses the first three principal components (PCs) as input variables for LDA, in which a 'leave-N-out' cross-validation technique has been used. The accuracy of the prediction method was evaluated

Biomedical Optics EXPRESS

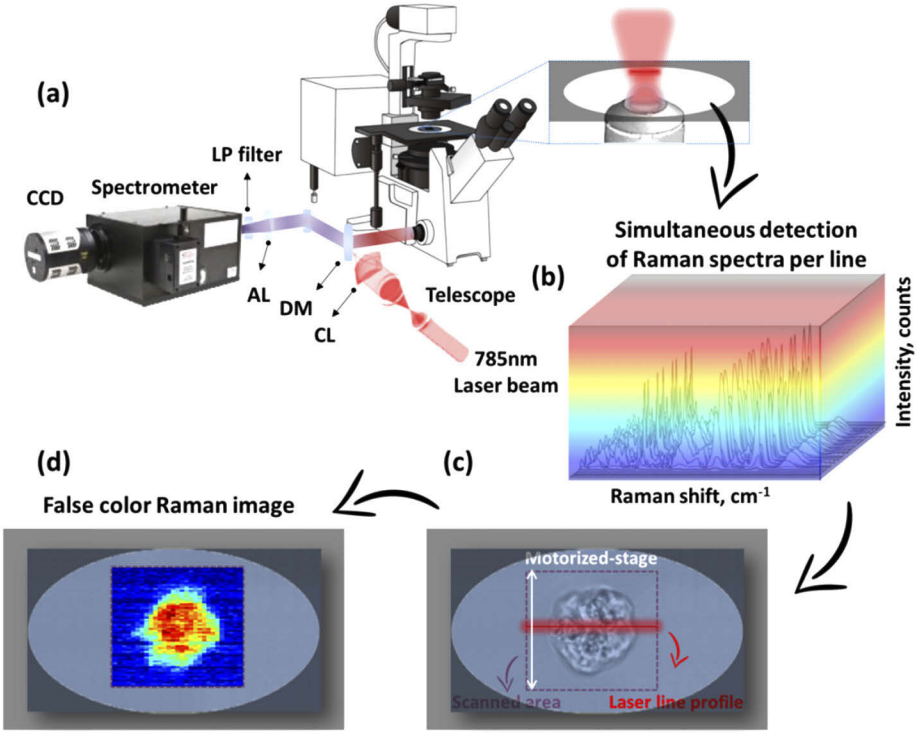

Fig. 1. (a) Line-scan hyperspectral Raman microscope: a 785 nm laser beam passes through a telescope and a cylindrical lens (CL) to generate the line-profile at the focus of the 60X water immersion microscope objective. A dichroic mirror (DM) separates the Raman signals from the excitation light. Raman signals, filtered by a longpass (LP) filter, are delivered through an achromatic lens (AL) into a spectrometer with a CCD detector. (b) The 100 vertical pixels of the CCD camera are used for simultaneous detection of Raman spectra along the line focus. (c) The motorized stage scans the cell perpendicular to the laser line profile to probe the Raman spectra of the entire cell area. (d) False color Raman images are generated for each cell by choosing a specific Raman peak of interest and using its band area intensity at each image pixel to create the image.

by using the confusion matrix. All homemade algorithms were written in Matlab (Mathworks, USA).

2.4. Statistical analysis

The performance of the developed PCA-LDA classification model was evaluated by using a confusion matrix, where cells where classified as true negative (TN), false positive (FP), true positive (TP) and false negative (FN). Sensitivity, specificity and diagnostic accuracy (DA) can then be calculated. Sensitivity is defined as the proportion of true positive (TP) subjects with the disease to the subjects classified, by the model, as having the disease (TP + FN). Similarly, specificity is defined as the proportion of subjects without the disease, with true negative (TN) test result, to the total subjects classified without disease (TN + FP). DA, [Eq. (1)], gives an overall measure for the efficiency of the model and is expressed as a proportion of correctly classified subjects among all subjects as follows:

$$DA = \frac{(\mathrm{TP} + \mathrm{TN})}{(\mathrm{TP} + \mathrm{TN} + \mathrm{FP} + \mathrm{FN})} \tag{1}$$

Biomedical Optics EXPRESS

3. Results

Figure 2 shows the average Raman spectra of 117 single cell spectra from 4 different MTC nodules. The shaded region represents ±1 standard deviation (SD) and dashed lines indicate the significant Raman peaks. Their corresponding biological assignments [15,16] are listed in Table 2.

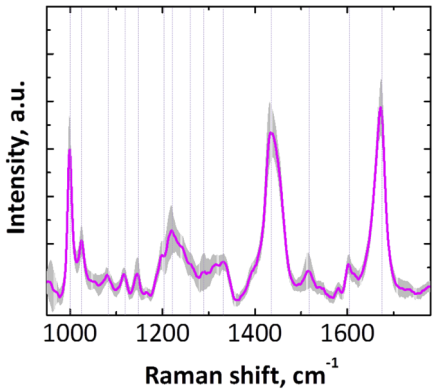

Fig. 2. Average Raman spectrum of 117 single cells from MTC nodules, with the shaded region representing ±1 SD.

Table 2. Raman peaks and their corresponding biological assignments.

Assignments	Raman Peak (cm^{-1})
Phenylalanine, protein	1003
Phenylalanine, protein, carbohydrate residues of collagen	1031
Phosphodiester groups in nucleic acids	1080
Carotene, C-O band of ribose (marker band for RNA)	1120
Carotenoid	1148
Phenylalanine, tryptophan, adenine and tyrosine (ring breathing), amide III	1205
Amide III (β sheet structure)	1224
Lipids	1260
Cytosine, lipid, collagen	1293
Nucleic acids, DNA, phospholipids	1330
Lipid	1430
Carotenoid stretching (C = C), cytosine	1516
Phenylalanine	1602
Amide I (proteins), protein band carbonyl stretching (C = O), lipid stretching	1667

We had previously reported on the single cell Raman signatures from benign nodular hyperplasia and classic variant of papillary thyroid carcinoma (CVPTC) [15]. Here, we compare the MTC cell spectra to the spectra of those cell types. Figure 3 shows representative single cell hyperspectral Raman images at the three highest intense Raman peaks (1003, 1430, and 1667 cm^{-1}), which show clear differences in their intensities for the three cell types. The full spectral differences between these cell types is better illustrated in difference spectra, generated by subtracting the average spectra of benign and CVPTC cells from the average spectra of MTC cells seen in Figs. 4(a) and 4(b), respectively. Vertical lines, as in Fig. 2, indicate the most relevant peaks in the difference spectra. For classifying and discriminating the cell groups, the full spectral data

Biomedical Optics EXPRESS

for all three cell types were used as input variables for PCA, which generated new variables, the PCs, which capture the maximum variance in the multidimensional data.

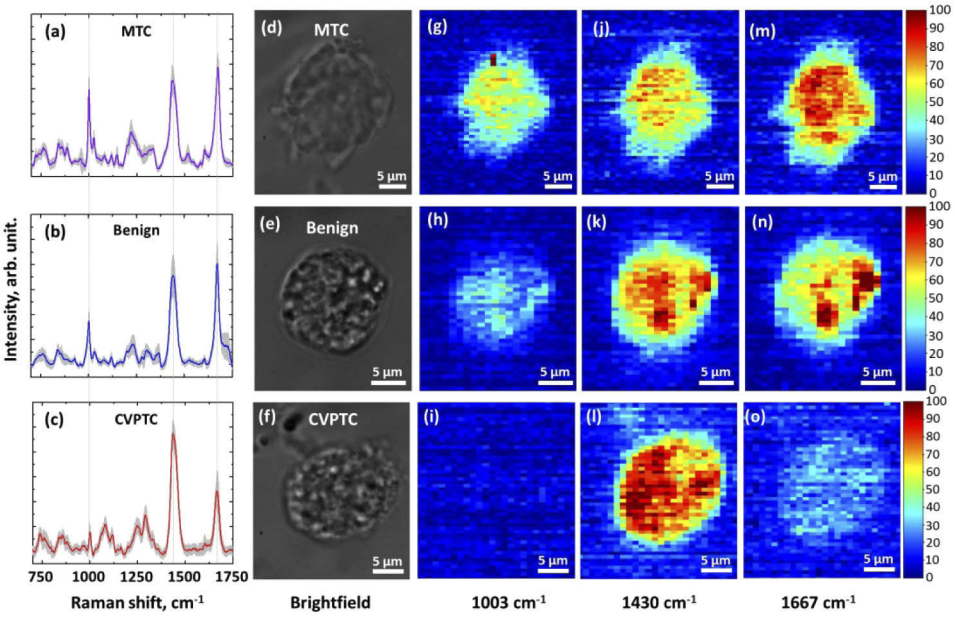

Fig. 3. Raman average spectra over (a) 117 MTC (magenta line), (b) 127 benign (blue line) and (c) 121 CVPTC (red line) cells. (d-f) Brightfield and (g-o) false color Raman images generated by using 1003 cm^{-1}, 1430 cm^{-1}, and 1667 cm^{-1} Raman bands.

PCA coefficients were used to compare MTC versus benign and MTC versus CVPTC cells. Figures 4(c) and 4(d) show the spectral contributions captured by the first principal component (PC1). In both instances, PC1 mirror quite well the difference spectra shown in Figs. 4(a) and 4(b) and capture 29% and 45% of the total data variance, respectively. The first three PCs together captured 57% and 59% of the total data variance, respectively. These three PCs were used as inputs in subsequent LDA analysis.

Figures 5(a) and 5(b) show 3D PCA-LDA plots of the covariance error ellipsoids, with 95% interval confidence. The results of a leave-N-out cross validation analysis generates confusion matrices, allowing the accuracy in discriminating MTC cells from benign and CVPTC cells to be quantified (Figs. 5(c) and 5(d)). A 95% DA, 96% sensitivity, and 95% specificity for discriminating MTC and benign cells was determined. For identifying MTC from CVPTC cells, these values were 98%, 99%, and 99%, respectively.

MTC cells, compared to both benign and CVPTC cells, have showed higher peak intensities at phenylalanine (1003, 1031 and 1602 cm^{-1}) and carotenoids (1148 and 1516 cm^{-1}). One peak that is significantly different for the three cell types is located at 1003 cm^{-1}. Based on this peak intensity, we can conclude that the MTC cells have the highest phenylalanine levels, followed by benign cells, and with CVPTC cells having the lowest levels. To assess whether phenylalanine Raman spectral marker at 1003 cm^{-1} alone could potentially be used as a diagnostic marker to identify MTC cells, we analyzed the DA, sensitivity, and specificity based only on this specific peak intensity. Histograms of the 1003 cm^{-1} peak intensity, distributed in ascending classes of fixed interval, for every cell in these three cell groups are shown in Fig. 6(a). Shown in Fig. 6(b) are the average peak intensities and standard deviations for each group. Both the average intensity and histogram plots indicate that MTC cells have the highest phenylalanine peak intensity. Using an LDA model based solely on this peak value and performing a leave-N-out cross validation, we

Biomedical Optics EXPRESS

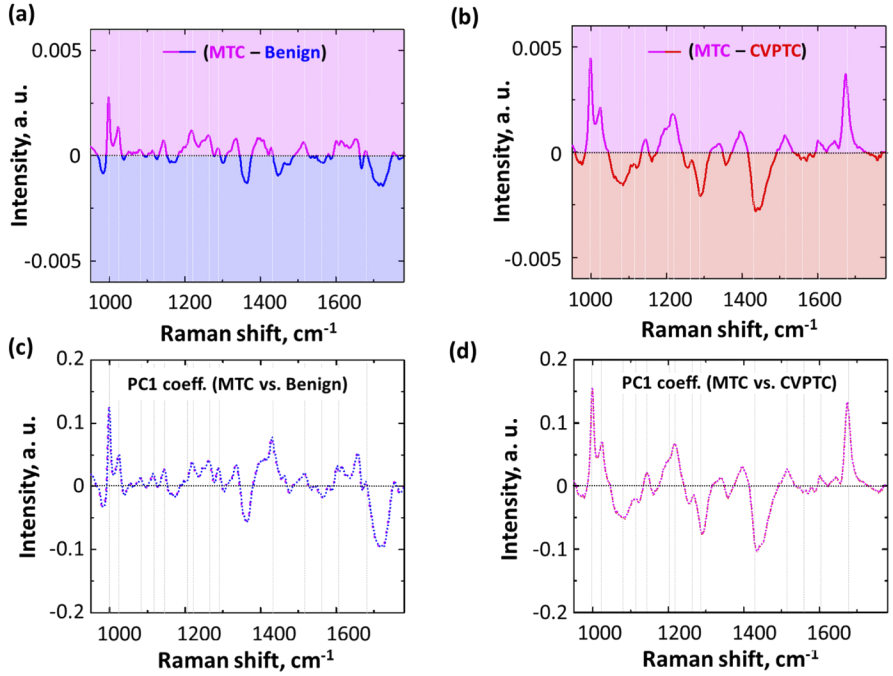

Fig. 4. Difference spectra generated by subtracting the average spectra of (a) benign and (b) CVPTC cells from the average spectra of MTC cells. Plot of the PC1 coefficients from PCA analysis of (c) MTC versus benign and (d) MTC versus CVPTC cells.

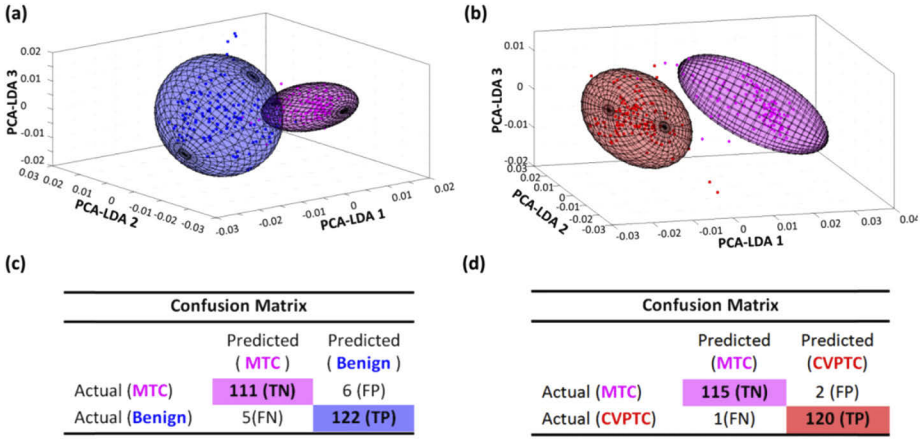

Fig. 5. PCA-LDA model for subtype classification. (a-b) 3D plots of 95% interval confidence covariance error ellipsoids and (c-d) confusion matrices for MTC versus benign and MTC versus CVPTC cells, respectively.

generated confusion matrices for the three different pairings, as shown in Fig. 6(c). MTC cells were differentiated from benign and CVPTC cells with 87 and 95% DA, respectively. Benign cells were discriminated from CVPTC cells with 79% DA.

Single cells from digested thyroid nodule tissues were utilized in this study. With the long term goal of developing "Raman-based cytopathology" on FNA samples as an ancillary test for indeterminate thyroid nodules, we set out to determine if the Raman signatures observed

Biomedical Optics EXPRESS

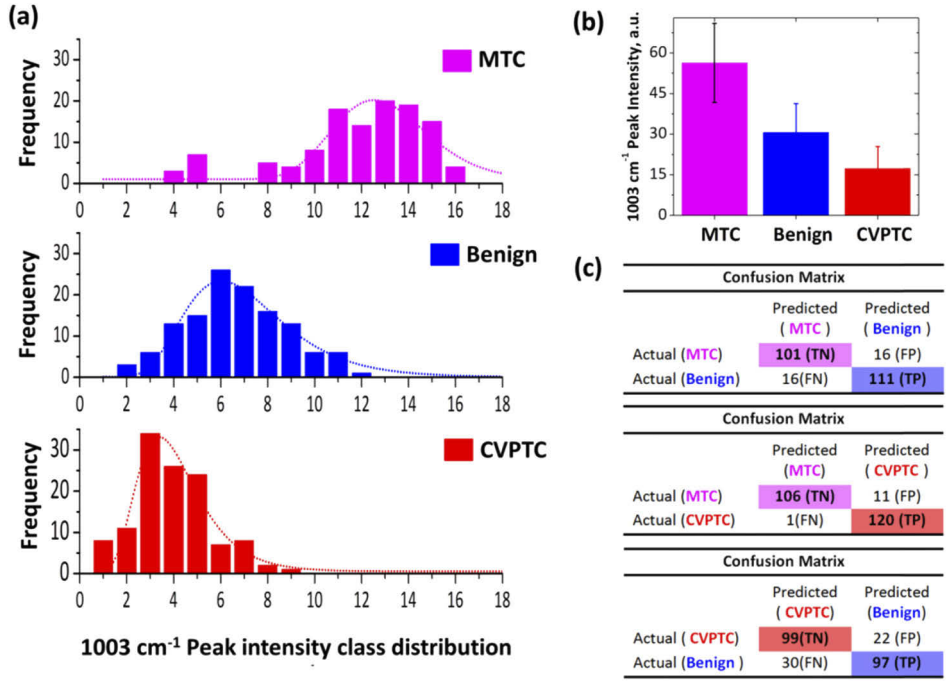

Fig. 6. (a) Histogram of the 1003 cm^{-1} peak intensity in class distribution for all 365 cells in the three cell groups. (b) Plot of the average peak intensity and ± 1standard deviation for each cell group. (c) Confusion matrices showing the cell classification results based on the 1003 cm^{-1} peak intensity.

in dissociated single cells are identical to cells that are obtained by FNA. Figure 7(a) shows the average spectra from cells that were obtained from MTC by the simulated FNA sampling (n=21) approach (see Materials and Methods), which is compared to the spectra of cells that were obtained by tissue digestion (n = 54) of the same MTC nodules. Also shown in Fig. 7(b) is a 2D PCA-LDA plot with 95% confidence interval that includes all data (i.e. digested MTC, benign and CVPTC cells and the FNA sampled MTC cells). MTC cells obtained by simulated FNA clearly cluster with the MTC cells that were obtained by tissue digestion. The results indicate that

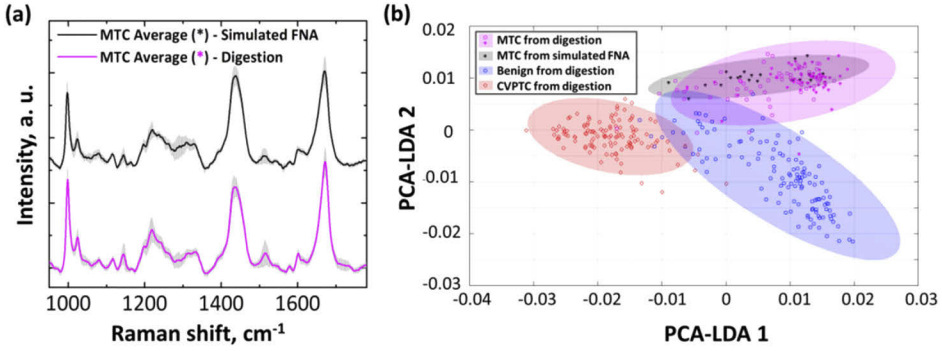

Fig. 7. (a) Offset average spectra of MTC cells obtained by FNA (n=21) and by tissue digestion (n=54), with the shaded region representing ±1 SD. (b) 2D PCA-LDA plots of all groups together with covariance error ellipses, with 95% interval confidence.

Biomedical Optics EXPRESS

the method used to digest thyroid tissue into isolated single cells does not alter the biochemical composition of these cells.

4. Discussion

Ultrasound-guided FNA is the first line diagnostic test for screening thyroid nodules and identifying patients who would benefit from surgical management. While FNA cytologic evaluation of some neoplasms, such as papillary carcinoma, is highly sensitive and specific, the detection rate for MTC remains a challenge [6]. Classic cytologic criteria for MTC include plasmacytoid or spindled cells, dyshesion, multinucleation, and "salt and pepper" chromatin. However, cytomorphology can be challenging when the sample is limited and not fulfilling all the cytologic criteria. In these indeterminate cases, ancillary testing such as calcitonin may be utilized as a confirmatory test; however, it has its own diagnostic pitfalls of false positive results [8]. Additionally, MTC has a tendency for regional lymph node metastasis at an early stage; therefore, MTC is occasionally diagnosed initially by FNA due to an enlarged cervical lymph node. Metastatic MTC in a lymph node can be diagnostically challenging, especially in FNA biopsies where tumor cells may be crushed with limited cytomorphology. In addition, metastatic MTC may lose the ability to express calcitonin, and the presence of TTF-1 immunohistochemical positivity may be misinterpreted as metastatic lung adenocarcinoma [17,18]. The clinical consequence of incorrect diagnosis is significant as clinical management differs significantly between metastatic MTC versus lung adenocarcinoma. In this clinical scenario, our single cell Raman-based cytopathology approach may prove to be a useful ancillary test by identifying MTC precisely using its unique Raman fingerprints, leading to correct treatment and management.

We recently reported using Raman spectral fingerprints to differentiate various thyroid nodules with high sensitivity and specificity [15]. In the current study, the spectra of MTC cells were compared to other nodules previously described, for the purposes of identifying unique spectral peaks that could potentially be used as a spectral biomarker for MTC diagnosis. While multivariate statistical methods were able to identify a combination of Raman peaks that, together, could accurately discriminate MTC from benign and CVPTC cells with 97% and 99% accuracy, one specific Raman peak (1003 cm^{-1}) known to be associated with phenylalanine was significantly different. When used alone for classification, this peak was able to identify MTC cells with 87% and 95% accuracy, respectively.

A recent study by Mun *et. al.* [19] using human C cells in culture showed that elevated extracellular calcium and phenylalanine concentration promotes calcitonin release acting via the calcium sensing receptor (CaSR). Since CaSR is positively modulated by L-amino acids, including L-phenylalanine, they also observed that calcitonin release increased with elevated levels of extracellular phenylalanine. In addition, Romero-Lluch *et. al.* demonstrated that 18-F-fluorodihydroxyphenylalanine, an amino acid analog used for positron emission tomography, is superior in detecting and locating recurrent MTC in patients [20]. Our findings are consistent with these observations and suggest that Raman spectroscopy may be detecting the elevated levels of phenylalanine in single cells of MTC thyroid nodules, which may play a role in the high calcitonin release that is very distinctive in MTC patients.

Cancer biomarkers are very helpful in clinical practice for diagnosis and treatment. Amino acids such as phenylalanine, tyrosine and tryptophan have been suggested as potential biomarkers of several malignancies [21]. Our current findings suggest, alternatively to calcitonin, phenylalanine would potentially be a new biomarker for MTC, and possibly other thyroid cancers. Phenylalanine is an essential amino acid found in a wide variety of foods, including plant and animal sources (e.g. mother's milk, meat, fish, eggs, and seeds). Phenylalanine is also the precursor of tyrosine, which is a nonessential amino acid that can be formed by the hydroxylation of phenylalanine and is metabolized to important substances in the body, such as neurotransmitters (epinephrine

Biomedical Optics EXPRESS

and norepinephrine) and plays an important role in the metabolism of the thyroid hormones [22]. Therefore, either the elevated level of phenylalanine observed in single cells of MTC or the diminished level in CVPTC may be indicative of alterations in phenylalanine-tyrosine metabolism in thyroid cancers.

We acknowledge that the current study has its limitation due to the small number of MTC nodules available for the study to draw a clinically strong conclusion. MTC is rare; therefore, it is not readily accessible. However, we were able to measure 138 single MTC cells from these nodules, and they all exhibited similar spectral fingerprints.

5. Conclusion

In conclusion, our data suggest that Raman spectroscopy is a potentially useful and powerful ancillary tool for MTC when current FNA cytopathology cannot provide a definitive diagnosis. The increase in phenylalanine levels detected by Raman spectroscopy is consistent with what is known about the biological process of calcitonin production and release in MTC. Also the changing in phenylalanine levels presented either by MTC or CVPTC nodules may be indicative of any alterations in phenylalanine-tyrosine metabolism in thyroid malignant pathway. In addition, MTC cells isolated from bench-top FNA yielded similar Raman signatures when compared to single cells digestion, suggesting that Raman-based hyperspectral cytopathology can be used as an adjunct technique to improve diagnostic accuracy of FNA cytology at a single cell level. It emphasizes even more that Raman-based cytopathology can potentially be used as an accurate supplementary diagnostic test to complement conventional FNA cytopathology. Also, with the discovery of specific spectral markers, such as 1003 cm^{-1}, providing high DA, Raman imaging methods (e.g. coherent anti-Stokes Raman scattering and stimulated Raman scattering) could potentially be implemented to reduce the acquisition time.

Acknowledgments

This work was supported by a Collaborative for Diagnostic Innovation Grant from the UC Davis Department of Pathology and Laboratory Medicine. Specimens were provided by the UC Davis Pathology Biorepository which is jointly funded by the UC Davis Comprehensive Cancer Center Support Grant awarded by the National Cancer Institute (NCI P30CA093373) and the UC Davis Department of Pathology and Laboratory Medicine. This work was also partially supported by a UC Davis Academic Senate Grant.

Disclosures

The authors declare no conflicts of interest.

References

1. C. Jimenez, M. I. N. Hu, and R. F. Gagel, "Management of medullary thyroid carcinoma," Endocrinol. Metab. Clin. North Am. **37**(2), 481–496 (2008).
2. E. Kebebew, P. H. G. Ituarte, A. E. Siperstein, Q. Y. Duh, and O. H. Clark, "Medullary thyroid carcinoma - Clinical characteristics, treatment, prognostic factors, and a comparison of staging systems," Cancer **88**(5), 1139–1148 (2000).
3. J. F. Moley, "Medullary thyroid carcinoma: management of lymph node metastases," J. Natl. Compr. Cancer Network **8**(5), 549–556 (2010).
4. E. Modigliani, R. Cohen, J. M. Campos, B. Conte-Devolx, B. Maes, A. Boneu, M. Schlumberger, J. C. Bigorgne, P. Dumontier, L. Leclerc, B. Corcuff, and I. Guilhem, "Prognostic factors for survival and for biochemical cure in medullary thyroid carcinoma: results in 899 patients. The GETC Study Group. Groupe d'etude des tumeurs a calcitonine," Clin. Endocrinol. **48**(3), 265–273 (1998).
5. E. S. Cibas and S. Z. Ali, "The 2017 Bethesda System for Reporting Thyroid Cytopathology," Thyroid **27**(11), 1341–1346 (2017).
6. P. Trimboli, G. Treglia, L. Guidobaldi, F. Romanelli, G. Nigri, S. Valabrega, R. Sadeghi, A. Crescenzi, W. C. Faquin, M. Bongiovanni, and L. Giovanella, "Detection rate of FNA cytology in medullary thyroid carcinoma: a meta-analysis," Clin. Endocrinol. **82**(2), 280–285 (2015).

Biomedical Optics EXPRESS

7. K. Kaserer, C. Scheuba, N. Neuhold, A. Weinhausel, O. A. Haas, H. Vierhapper, and B. Niederle, "Sporadic versus familial medullary thyroid microcarcinoma - A histopathologic study of 50 consecutive patients," American J. Surg. Path. **25**(10), 1245–1251 (2001).
8. S. P. A. Toledo, D. M. Lourenco, M. A. Santos, M. R. Tavares, R. A. Toledo, and J. E. D. Correia-Deur, "HYPERCALCITONINEMIA IS NOT PATHOGNOMONIC OF MEDULLARY THYROID CARCINOMA," Clinics **64**(7), 699–706 (2009).
9. Z. W. Baloch, E. S. Cibas, D. P. Clark, L. J. Layfield, B. M. Ljung, M. B. Pitman, and A. Abati, "The National Cancer Institute Thyroid fine needle aspiration state of the science conference: a summation," CytoJournal **5**(1), 6 (2008).
10. H. Abramczyk, M. Kopec, and M. Jedrzejczyk, "Raman Spectroscopy, Medical Applications: A New Look Inside Human Body With Raman Imaging," in *Encyclopedia of Spectroscopy and Spectrometry*, 3rd Edition, Vol 3: N-R, J. C. Lindon, G. E. Tranter, and D. W. Koppenaal, eds. (Academic Press Ltd-Elsevier Science Ltd, London, 2017), pp. 915–918.
11. H. Noothalapati, K. Iwasaki, and T. Yamamoto, "Biological and Medical Applications of Multivariate Curve Resolution Assisted Raman Spectroscopy," Anal. Sci. **33**(1), 15–22 (2017).
12. Z. A. Nima, A. Biswas, I. S. Bayer, F. D. Hardcastle, D. Perry, A. Ghosh, E. Dervishi, and A. S. Biris, "Applications of surface-enhanced Raman scattering in advanced bio-medical technologies and diagnostics," Drug Metab. Rev. **46**(2), 155–175 (2014).
13. A. Sahu, P. Gera, A. Malik, S. Nair, P. Chaturvedi, and C. M. Krishna, "Raman exfoliative cytology for prognosis prediction in oral cancers: A proof of concept study," J. Biophotonics **12**(8), e201800334 (2019).
14. D. Traynor, S. Duraipandian, R. Bhatia, K. Cuschieri, C. M. Martin, J. J. O'Leary, and F. M. Lyng, "The potential of biobanked liquid based cytology samples for cervical cancer screening using Raman spectroscopy," J. Biophotonics **12**(7), e201800377 (2019).
15. M. A. S. De Oliveira, M. Campbell, A. M. Afify, E. C. Huang, and J. W. Chan, "Hyperspectral Raman microscopy can accurately differentiate single cells of different human thyroid nodules," Biomed. Opt. Express **10**(9), 4411–4421 (2019).
16. Z. Movasaghi, S. Rehman, and I. U. Rehman, "Raman spectroscopy of biological tissues," Appl. Spectrosc. Rev. **42**(5), 493–541 (2007).
17. M. P. Pusztaszeri, M. Bongiovanni, and W. C. Faquin, "Update on the Cytologic and Molecular Features of Medullary Thyroid Carcinoma," Adv. Anat. Pathol. **21**(1), 31–40 (2014).
18. K. S. Wong and J. A. Barletta, "Thyroid Tumors You Don't Want to Miss," Surg. Path. Clin. **12**(4), 901–919 (2019).
19. H. C. Mun, K. M. Leach, and A. D. Conigrave, "L-Amino Acids Promote Calcitonin Release via a Calcium-Sensing Receptor: G(q/11)-Mediated Pathway in Human C-Cells," Endocrinology **160**(7), 1590–1599 (2019).
20. A. Scarsbrook, S. Vaidyanathan, F. Chowdhury, S. Swift, R. Cooper, and C. Patel, "Efficacy of qualitative response assessment interpretation criteria at 18F-FDG PET-CT for predicting outcome in locally advanced cervical carcinoma treated with chemoradiotherapy," Eur. J. Nucl. Med. Mol. Imaging **44**(4), 581–588 (2017).
21. T. Wiggins, S. Kumar, S. R. Markar, S. Antonowicz, and G. B. Hanna, "Tyrosine, Phenylalanine, and Tryptophan in Gastroesophageal Malignancy: A Systematic Review," Cancer Epidemiol., Biomarkers Prev. **24**(1), 32–38 (2015).
22. G. Litwack, "Chapter 13 - Metabolism of Amino Acids," in *Human Biochemistry*, G. Litwack, ed. (Academic Press, Boston, 2018), pp. 359–394.